energies

MDPI

Article

Step-Up DC-DC Converter Supplied by a Thermoelectric Generator for IoT Applications

José Almeida [1], P. Mendonça dos Santos [1,2], João Caldinhas Vaz [2,3], Ricardo A. Marques Lameirinhas [2,3,*], Catarina Pinho Correia Valério Bernardo [2,3] and João Paulo N. Torres [2,3]

[1] Academia Militar/CINAMIL, Av. Conde Castro Guimarães, 2720-113 Amadora, Portugal; almeida.jcs@gnr.pt
[2] Instituto de Telecomunicações, 1049-001 Lisbon, Portugal; pms@lx.it.pt (P.M.d.S.); joaovaz@tecnico.ulisboa.pt (J.C.V.); catarina.bernardo@tecnico.ulisboa.pt (C.P.C.V.B.); joaoptorres@hotmail.com (J.P.N.T.)
[3] Department of Electrical and Computer Engineering, Instituto Superior Técnico, 1049-001 Lisbon, Portugal
* Correspondence: ricardo.lameirinhas@tecnico.ulisboa.pt

Abstract: This research work aims to design and prototype a DC-DC converter to step up the low voltage of a small, low-power thermoelectric generator (TEG). The system is based on an inductive boost converter and attains a regulated output voltage of 1.2 V. The design's optimisation was based on simulation and experimental validation and it was implemented with only ten low-cost commercial off-the-shelf (COTS) components. To reduce complexity, the low-side switch MOSFET of the boost converter is directly driven by an LC oscillator, switching at 1.25 MHz. For loads above 20 kΩ, the converter ensures voltages higher than 1.2 V, supplied by the TEG voltage of 0.5 V, while registering identical efficiency values to those of more complex and expensive CMOS-integrated solutions. These designed features suggest applications in remote IoT nodes and portable devices, delivering sufficient power to backup the supply of corresponding sensing and communication low-power circuits, reducing the necessity of battery replacements or increasing their lifetime.

Keywords: energy harvesting; thermoelectric generator; boost converter; commercial off-the-shelf components

Citation: Almeida, J.; Mendonça dos Santos, P.; Caldinhas Vaz, J.; Marques Lameirinhas, R.A.; Pinho Correia Valério Bernardo, C.; Torres, J.P.N. Step-Up DC-DC Converter Supplied by a Thermoelectric Generator for IoT Applications. *Energies* **2024**, *17*, 5288. https://doi.org/10.3390/en17215288

Academic Editors: Hervé Morel, Mahmoud Bourouis, Nadjet Zioui, Peter Breuhaus and Said Bentouba

Received: 26 August 2024
Revised: 17 October 2024
Accepted: 22 October 2024
Published: 24 October 2024

1. Introduction

The idea of the IoT (Internet of Things), where devices with embedded electronics, sensors, actuators, and software are connected and interact over the internet, has gained widespread attention [1]. Wearable technology is also an area of growing interest for personal health monitoring and the incorporation of various electronic sensors. A combination of the IoT and "wearables" can improve quality of life by reducing the cost of [2] healthcare, as well as monitoring daily training and performance.

Thermoelectric generators, TEGs, and photovoltaic cells are some of the most promising Energy Harvesting (EH) sources for very-low-voltage and -power applications.

A thermoelectric generator (TEG) is a device that produces electrical energy from the temperature difference between two plates. This technology was discovered by Thomas Johann Seebeck in 1821. According to Seebeck, it is possible to obtain a difference in electrical potential by applying a difference in temperature to two types of material. As a result, this phenomenon is known as the 'Seebeck effect' [3].

In the past, TEGs used metallic thermoelectric materials, while more recently manufactured TEGs use alternating n- and p-type semiconductor materials. The structure of a TEG is a stack or sandwich, with thermoelectric materials used as the two heat exchanger plates at either end. A high temperature is applied to one of the two plates, called the 'hot' side of the TEG, while the other plate has a lower temperature and is called the 'cold' side of the TEG [3]. The typical structure of a TEG is illustrated in Figure 1.

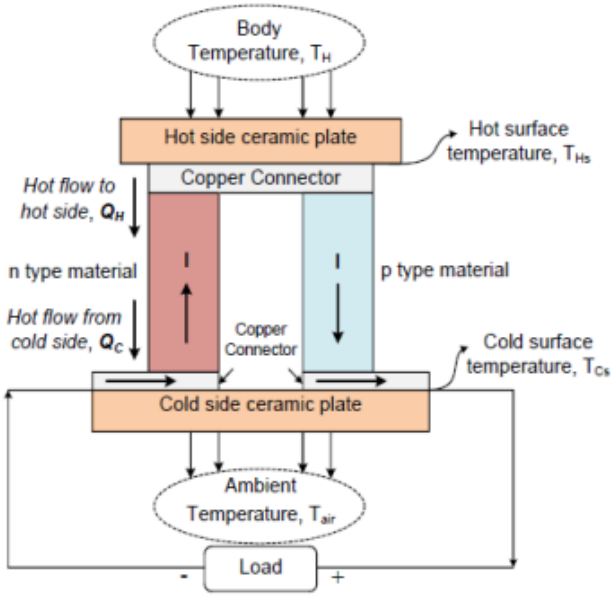

Figure 1. Typical TEG structure (from [3]).

The TEG's output power and voltage generally range from a few μW to 10 mW and from 50 to 600 mV, respectively. The actual values depend on the temperature difference and size of the TEG [4].

To power a battery or IoT device, it is necessary to convert the output voltage of the TEG to a standard output voltage (1.2 V, 2.4 V, 3.3 V, or 5 V).

This research work aims to design and prototype a DC-DC converter to step up the low voltage of a low-power thermoelectric generator. Theoretical and simulation tests are carried out before experimental realisation with only commercial off-the-shelf (COTS) components. Thus, we are showing a low-cost solution, without the necessity of application-specific and low-volume CMOS integration and with a reasonable efficiency and area occupation. The goal is to step-up a TEG voltage of hundreds of mV to a regulated voltage of 1.2 V, delivering enough power to the load/battery for remote IoT communication and sensing purposes, together with portable devices for wearable applications [5]. The key idea is not to replace the battery. Instead, the system should deliver enough power to reduce the necessity of battery replacements and to increase its lifetime.

2. Background Research and State-of-the-Art Systems

Several topologies are being proposed, considering different approaches, to realise the converter and each functional block.

The reported works present variations that improve the performance of the converter, raising the output voltage as much as possible and minimising the input voltage. For example, the work in [6] shows a solution with photovoltaic and thermoelectric harvesting based on commercial power-conversion-dedicated integrated circuits. Although it is already possible to use commercial converters to power IoT nodes, different solutions are being reported, aiming to improve the system's overall performance or specific features, like area minimisation or component count reduction. Some of these systems require an external source for their start-up like a piezoelectric actuator [7,8]. Throughout the analysis, one notices that the developed systems often feature maximum power point tracking (MPPT), control circuits, and the use of transformers to start up the circuit [9–11]. Also, in [12], the authors propose an hybrid, reconfigurable, and battery-assisted system, with the complex part of the converter control and start up integrated into a 65 nm CMOS component, achieving an output voltage of 1.4 V. The circuits presented in [13,14] are also

based on the classical inductor boost topology, but their start-up process is assisted by charge pump circuits.

Table 1 presents several step-up converters' topologies proposed within the scope of energy harvesting with TEGs. The parameters under analysis for comparing the different typologies are the input and output voltage, the switching frequency, the efficiency, the manufacturing process, the architecture of the step-up DC-DC converter, and the circuit-specific power supply. Other specifications related to their area occupation like their silicon footprint and power density are not comparable features with this work, since our proposal is based on a COTS printed circuit board prototype.

The authors of [10] present a two-stage DC-DC step-up converter. Like in the work proposed in [9], this circuit is based on the transformer-based operating mode (TOM) concept. It includes a control system with MPPT and starts with a minimum input voltage of 20 mV, attaining 1.2 V at its output. Other works using a transformer with a flyback topology are reported in [15,16] and have a start-up circuit based on a JFET LC oscillator. These proposals are designed with COTS components except for their high-volume coils.

The circuit presented in [13] is based on the charge pumping topology, with a start-up added by a ring oscillator. The system operates at a minimum input voltage of 57 mV, and can be powered by a high-area TEG with a temperature gradient of less than 2 °C.

In [14], a DC-DC voltage boost converter is proposed that is a cold starter based on an ultra-low-power oscillator, a charge pumping scheme, and a zero-current switching circuit, which allows its start-up voltage to be very low (11 mV).

Ref. [17] proposes a ring oscillator and a flyback topology to step up the TEG voltage, ensuring 1.1 V at the output with a start-up voltage of around 60 mV.

Ref. [18] presents a low-cost COTS solution to step the TEG voltage up to 3 V using a hard-switch inductor-based boost converter switching at the very low frequency of 1 kHz.

Finally, the work proposed in [19] also suggests a hard-switch inductor-based boost converter with some additional circuitry activated by a cold-start ring oscillator to attain a maximum of 1.2 V using a 190 mV start-up voltage.

Table 1. Comparison of different voltage-boosting DC-DC converter topologies used in energy harvesting.

References	[10]	[13]	[14]	[17]	[18]	[19]
Year	2019	2019	2020	2024	2020	2019
V_{in} [V]	0.038	0.057	0.011	0.06	0.2	0.19
V_{out} [V]	1.2	-	0.8	2.72	3	1.2
Frequency	80 kHz	25 kHz	3.9 MHz	1.2 MHz	1 kHz	-
Efficiency [%]	81.5	-	85	72	-	60
Process	CMOS 180 nm	CMOS 180 nm	CMOS 130 nm	-	-	CMOS 180 nm
Architecture	Transformer-based oscillating mode (TOM)	Inductive boost with charge pump and ring oscillator as cold starter	Inductive boost with charge pump as cold starter	Flyback	Inductive boost	Inductive boost with ring oscillator as cold starter
Source	TEG	TEG	TEG	TEG	TEG	TEG

As can be seen from the inspection of the contributions presented in Table 1, almost all works resort to an inductor-based boost converter to step up the voltage obtained from the TEG.

The works presented in [10,13,14,19] are mainly based on expensive CMOS-integrated chip fabrication. Although two references [17,18] suggest a discrete COTS printed circuit board solution, only [18] focuses on cost reduction.

The present proposal aims to step up the voltage of a low-area and low-power TEG to an unregulated voltage above 1.2 V using a hard-switch inductor-based boost converter. The focus is on reducing the overall system cost and component count by using multiple devices' surface-mount technology packages together with a mature and low-power semiconductor driving strategy.

3. Thermoelectric Generator

The working principle of a TEG is based on the Seebeck effect. Considering a certain reference voltage, the Seebeck coefficient (S) of a certain material represents the voltage generated per degree of temperature variation (V/K). Each material is characterised intrinsically by this coefficient. TEGs with only one material are possible, namely with metals. However, recent technologies have resorted to n- and p-type semiconductors in order to improve the Seebeck coefficient in terms of its magnitude and linearity.

Equation (1) shows the relationship between the temperature variation and the generated open-circuit voltage (V_{oc}). Globally, this is not a linear relation. However, the device's operation is linear within a certain temperature range.

$$V_{oc} = \int_{T_c}^{T_h} S_n(T) - S_p(T) dT \rightarrow V_{oc} = S\Delta T \quad (1)$$

A commercial TEG was selected for this research work. A low-power and low-voltage TEG was chosen in order to justify this research. The difficulty is the designing of a DC-DC converter suitable for this low-voltage (under 1 V) application.

A MGM250-17-10-16 (Mini Thermoelectric Generator Module from Adaptive Power Management) was chosen due to its relatively small dimensions: 1.1 × 1.1 cm^2 (1.21 cm^2). We intended to consider T_h = 250 ºC and T_c = 30 ºC. The objective is to consider a cold plate temperature between 25 and 30 ºC and a variable hot plate temperature below a maximum of 250 ºC. For that range of temperatures, the TEG's internal resistance takes a value of 1 Ω and its match load condition imposes an output voltage below 0.65 V.

Figure 2 presents the Simulink model of a TEG. It denotes the linear dependence of the open-circuit voltage as a function of the input temperature difference ($\Delta T = Th - Tc$), as according to Equation (1). The Seebeck block returns the value of the coefficient S, considering the proposed temperature and working voltage ranges. This value is multiplied by the temperature difference (the model's input). Furthermore, since thermoelectric modules may be placed in series, the generated voltage may be multiplied by a given number of modules. According to the datasheet, a series resistance is also presented in the model to denote ohmic and contact voltage losses. This voltage is available in a differential terminal.

Using this model, several simulations were performed. Figure 3 shows the TEG's matched-load voltage as a function of the hot plate's temperature variation, considering the cold plate at the labelled values.

The TEG was also experimentally characterised under matched-load conditions. Figure 4 shows its output voltage for T_h = 230 ºC. Since it is impossible to instantaneously heat the plate, this figure represents the voltage variation considering a temperature increase between the room temperature and the desired value. However, when comparing the experimental results with the simulated ones, there are no significant differences between the simulation at T_c = 30 ºC and the experimental procedure considering T_c = 25 ºC. For these stimuli, the TEG generates a maximum voltage of 600 mV.

This value is scarcely enough to power up even a common low-voltage electronic device. Several TEGs may be connected in series in order to increase the voltage at the same operating temperature. Another perspective is the possibility of reducing the temperature difference in proportion to the number of added TEGs. Nonetheless, the focus of this work is to use just one TEG and to increase the available voltage by the use of a DC-DC step-up converter.

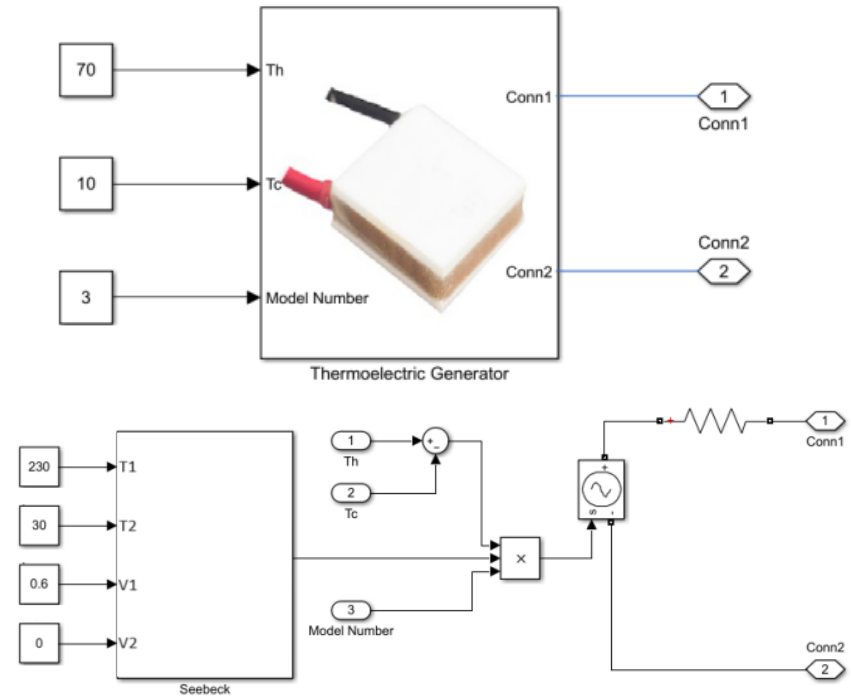

Figure 2. TEG electrical model, showing the block-view macro on top and the corresponding model at the bottom.

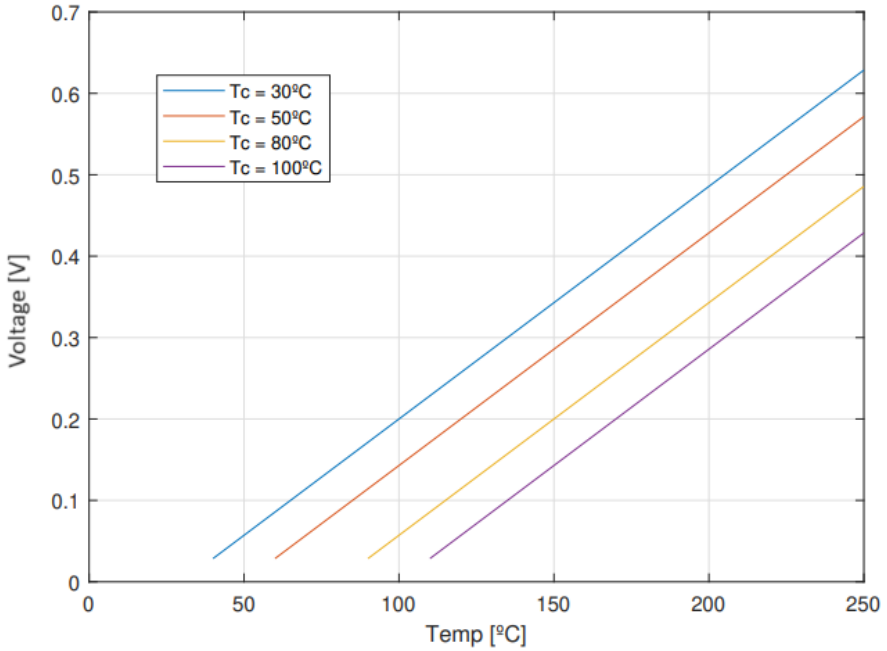

Figure 3. The TEG's characteristic output voltage curve for a matched-load condition, as a function of the hot plate temperature, for different cold plate temperatures (30 ºC, 50 ºC, 80 ºC, and 100 ºC).

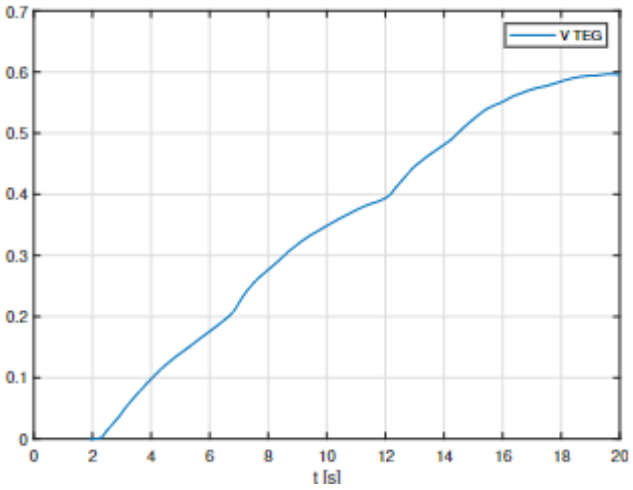

Figure 4. The TEG's output voltage variation over time for matched-load conditions and a final hot plate temperature of 230 ºC.

4. Harvesting System Design

This section aims to present the design methodology used to achieve an output voltage higher than the standard value of 1.2 V while considering a resistive load. The design was based on the fundamental equations and well-known electrical performance of an inductor-based DC-DC boost converter, together with simulations taking into account the almost ideal behaviour of the semiconductor devices. To ensure the system started up with the low-voltage obtained from the TEG, all the MOSFETs in the system were considered to have a null-threshold voltage. Also, the losses on the Schottky diode were considered to be constant and below 0.2 V. The Simulink schematic of the entire harvesting system is illustrated in Figure 5.

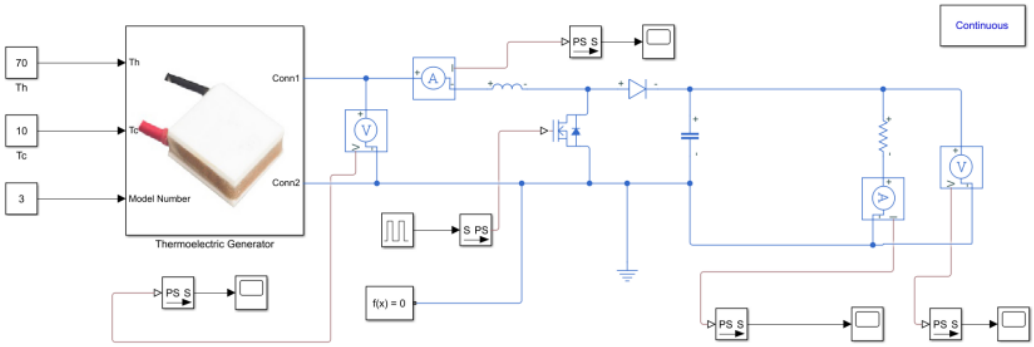

Figure 5. Schematic of the entire harvesting system, showing the TEG supply of the DC-DC boost converter.

As aforementioned, the goal of this work is to reduce the component count of the COTS components used. Therefore, the maximisation of the DC-DC conversion ratio is within our scope for such a low-voltage TEG supply. Since the component count of the boost converter cannot be reduced, we must focus on the driven circuit of the low-side MOSFET switch. In this scenario, it is impossible to design a MOSFET-driven circuit based, for example, on Operational Amplifiers, since there is no room for a supply with a TEG voltage below 1 V. In addition, other oscillator solutions like the ring oscillator are prone to excessive power consumption. Therefore, a simple Colpitts LC oscillator was designed to drive the boost converter's low-side switch. The direct consequence is that the driving signal will not be a square wave. Instead, the oscillator must be designed in order to achieve a saturated sine wave.

In order to maximise the DC-DC conversion ratio, the boost converter should operate in its Discontinuous Conduction Mode (DCM). Nonetheless, one may also take into consideration the fact that due to the non-ideal MOSFET-driven conditions, the output voltage will be lower than that obtained through classical boost equations (which assumes an ideal square-wave drive condition).

The oscillator is illustrated in Figure 6. It consists of an LC-tuned tank and a common-source amplifier. The oscillator was designed for a switching frequency, f_s, of 1.2 MHz, with a minimum voltage supply of 0.2 V, considering the MOSFETs' parasitic capacitance c_{cg}, because they are not negligible as the used capacitors have identical values. Thus, according to [20], the oscillator's feedback loop was sized to L = 470 µH, R = 1.2 kΩ, C_1 = 10 pF, and C_2 = 47 pF.

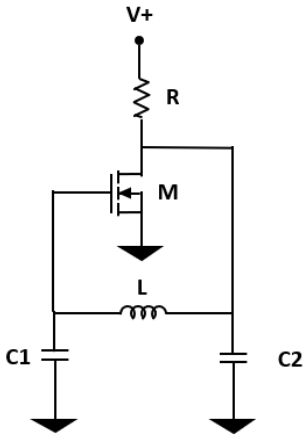

Figure 6. Schematic of Colpitts LC oscillator.

Having designed the oscillator, one may attempt to design the boost converter. The objective is to ensure an output voltage above the standard value of 1.2 V. For harvesting purposes, the size goal is to ensure voltages above 1.2 V in DCM for input voltages higher than 0.4 V, with 0.1 V of tolerance for input variations.

Based on these conditions and according to Expression (2), for a load resistance of 20 kΩ, the boost inductor (L_b) must take the standard value of 150 µH, considering the 50% duty-cycle (D) of the aforementioned LC oscillator [20].

$$V_o = \frac{V_i}{2} + \frac{V_i}{2}\sqrt{1 + \frac{2\,D^2\,R_L}{2\,f_s\,L_b}} \tag{2}$$

For the boost converter operating in DCM, the output voltage ripple can be defined by Equation (3). According to the previously designed values, the output capacitor (C_b) was computed to have 4.7 nF to ensure a ripple of around 1%.

$$\Delta V_o = \frac{V_o}{R_L\,f_s\,C_b}\left(1 - \sqrt{\frac{2L_b\,f_s}{R_L}}\right) \tag{3}$$

Figure 7 shows the voltage output (*vout*) when the converter is supplied with a TEG voltage of 0.5 V, with a conversion ratio of nearly 2.6. Also, as can be seen by the inductor current waveform, the converter is operating in DCM. Moreover, the simulation validates the MOSFET driving of the LC oscillator (*vosc*).

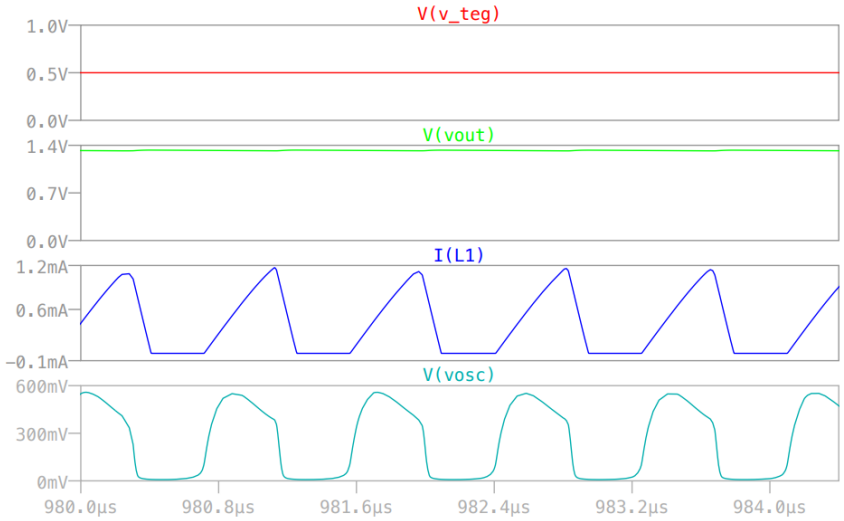

Figure 7. Simulated waveforms of the boost converter supplied by the TEG. From top to bottom: the TEG supply voltage, boosted output voltage, boosted inductor current, and MOSFET driving voltage.

5. Prototype Design with Commercial Off-the-Shelf Components

The main challenge in this work is starting up the boost converter and the oscillator with voltages below 1 V while prioritising component count and miniaturisation. According to these constraints, thorough component selection is in order; namely, field effect transistors with a nearly null-threshold voltage and low-on-voltage Schottky diodes, under low-profile surface-mount technology (SMT), should be chosen.

5.1. Semiconductor Device Selection

The TEG ensures a boost input voltage of the order of 0.5 V. However, standard the MOSFET threshold voltage is above this value. Thus, this work is based on MOSFETs with Vth = 0 V $\pm$ 0.02 V, which are used for ultra-low-power circuits.

The ALD212900SAL integrated circuit (IC) package was selected, which includes two n-channel transistors suitable for the minimisation of the component count, since only two MOSFET are needed (one for the oscillator and the other for the boost converter's low-side switch).

Taking into account the input voltage of 0.5 V and output voltage of 1.2 V required in this work, the silicon diode is no longer a viable option, as it requires a voltage drop above 0.5 V to conduct. This makes it necessary to use Schottky diodes, since their on-state voltage drop is around 0.2 V. Furthermore, Schottky diodes also perform well at the MHz switching frequency range. Based on these facts, the RB717UM diode was chosen.

5.2. Low Dropout Regulator

The TPS7A0512PDBZT was the voltage regulator selected due to its relatively small size (1.2 mm $\times$ 2.8 mm) and the required nominal voltage. This low dropout (LDO) regulator generates 1.2 V for an input range between 1.3 V and 5.5 V. Furthermore, it consumes a typical ultra-low quiescent current of 1 µA, making it suitable for harvesting applications.

5.3. Supercapacitor

This work proposes an innovative solution to circumvent the sporadic availability of high temperatures on the TEG hot plate. In fact, as confirmed experimentally, the TEG output voltage drops below 0.4 V within a few seconds after the removal of the heat source. To maximise the time that the system's output voltage is above 1.2 V, a supercapacitor (SC) is placed in parallel to the TEG. In this way, the system will deliver power to the load for a longer time period, enabling the operation of remote systems for extended periods of time.

5.4. Design of the Final Prototype

The system's printed circuit board (PCB) was sized while bearing in mind the smallest possible area to accommodate the COTS components. The PCB was fabricated with a double layer, as can be seen in Figure 8. In this way, a minimised PCB area of 1.5 cm × 1.6 cm was found to be adequate for the COTS components, and an equivalent area was reserved for the SC's placement.

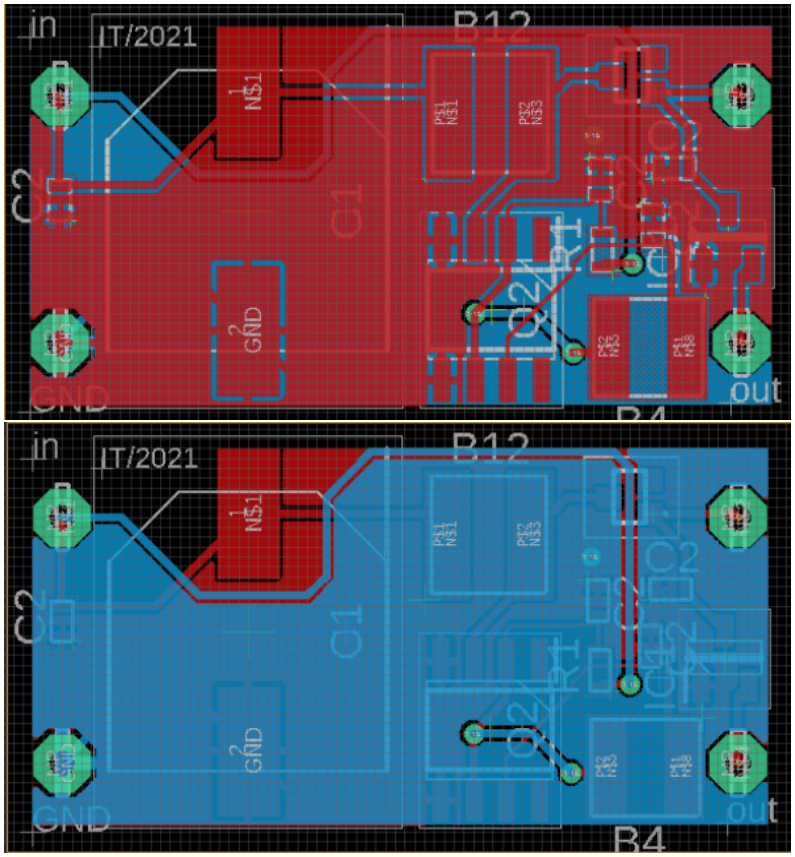

Figure 8. Printed circuit board: top view and bottom view.

Figure 9 shows the final prototypes of the boost converter with and without a supercapacitor. The circuit has a small footprint of 2.4 cm^2, and its area is doubled when including the supercapacitor.

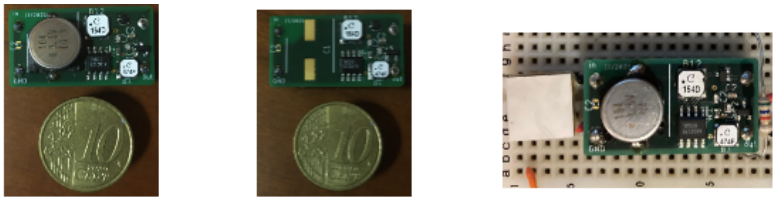

(a) (b) (c)

Figure 9. Final PCB of the boost converter (**a**) with the SC and (**b**) without the SC; (**c**) the full system with the SC powered by a TEG.

6. Experimental Results

6.1. Oscillator

The first circuit to be analysed is the oscillator. Its start up definitely influences the boost converter's performance. The oscillator's voltage waveform is first measured, considering a DC voltage source.

Figure 10 (left) shows the experimental waveform of the oscillator, highlighting the fact that it has an oscillation frequency of 1.25 MHz, which is very close to the intended specifications for a duty-cycle of approximately 50%. This is verified for a 20 kΩ load and an input voltage of 0.5 V and, as can be seen, the output voltage is above 1 V. As presented in Figure 10 (right), the boost converter has a start-up time of nearly 150 µs.

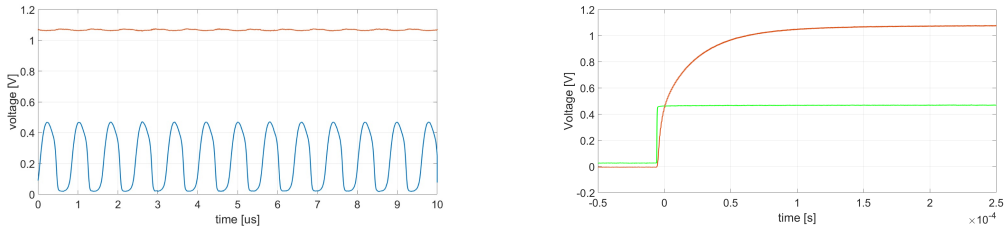

Figure 10. The steady-state boost output voltage (red) and oscillator voltage (blue) are illustrated on the left, while the transient of the boost output voltage (red) and the supply voltage (green) are shown on the right.

As can be seen in Figure 11 (left), the LC oscillator starts with a system input voltage below 180 mV. However, the oscillation voltage's swing is not enough to properly switch the boost MOSFET into its cut-off state. Figure 11 (right) shows the oscillator output and MOSFET drive voltage for a system supply of 220 mV. In this condition, the boost circuit operates with a conversion ratio below 1, limited by the voltage drop at the Schottky diode. It was also found experimentally that to double the input voltage, the system must be supplied with a minimum of 280 mV.

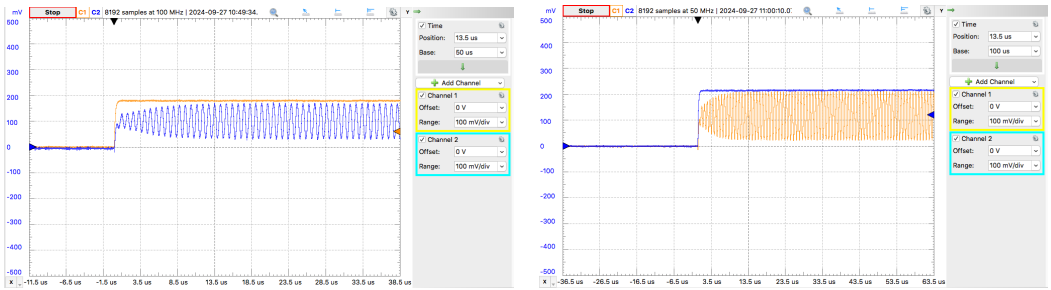

Figure 11. Oscillator start-up for system input voltages of 180 mV (**left**) and 220 mV (**right**).

6.2. Step-Up DC-DC Converter

Figure 12 presents the DC-DC conversion characteristic of different load values. It is possible to conclude that the higher the resistance, the higher the output voltage, as expected by Equation (2). It is possible to conclude that, for inputs in the range of 0.5 V–0.6 V, the minimum load resistance that ensures 1.2 V is 20 kΩ. As can be confirmed in the figure, the minimum voltage needed to deliver power to the load is 180 mV, which is almost independent from the load value.

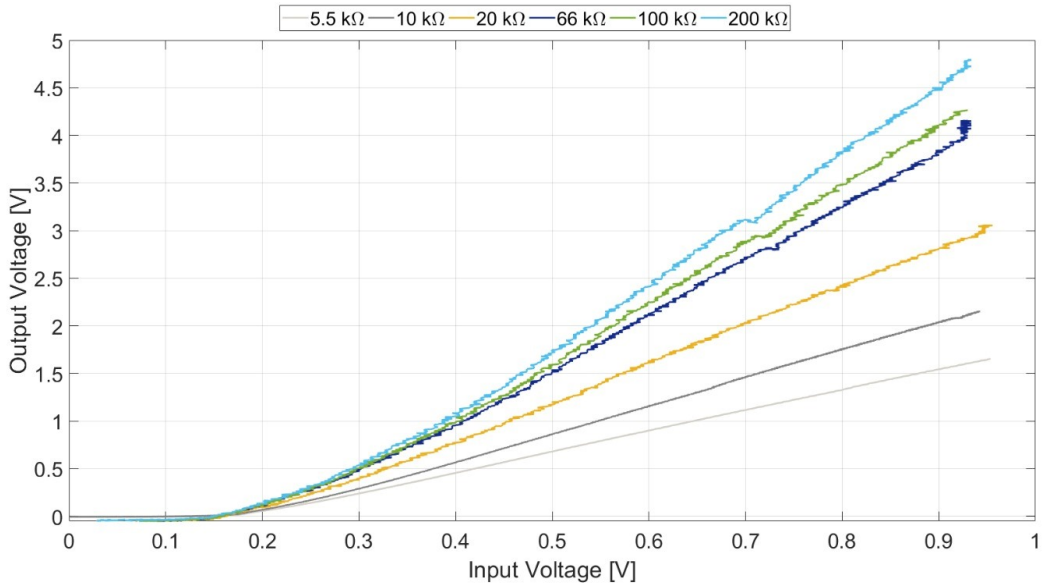

Figure 12. DC-DC conversion characteristics of different loads.

Besides the determination of the conversion characteristics, one may also be interested in computing and comparing the device's converter efficiency. Table 2 summarises the findings for different loads and input voltages. The experimental efficiency, η, was obtained by the measurement of the average input and output current and input and output voltage and corresponds to the ratio of the output power delivered to the load to the system's input power (needed to supply both the boost and the LC oscillator circuits). The conversion efficiency takes values between 17% and 74.6%, with the maximum obtained for a 5.5 kΩ load. Furthermore, the delivered power ranges from a dozen µW to mW, which is already reasonable for common electronic purposes, power sensing, and communication devices in IoT nodes or wearable systems. This is discussed in the next section.

Table 2. Converter efficiency and output power with different inputs and load values.

R [kΩ]	V_i [V]	V_o [V]	I_i [mA]	η [%]	P_o [µW]
20	0.5	0.96	0.55	17.0	46.08
	1.0	2.71	1.20	30.3	367.2
66	0.5	1.36	0.51	28.0	28.02
	1.0	3.93	1.10	21.3	234.0
5.5	1.0	1.51	1.10	42.0	414.6
	1.5	2.40	1.80	58.0	1047
	2.0	3.20	2.49	74.6	1862

6.3. System Analysis: TEG+Converter+LDO

After the boost converter's characterisation, the system's performance is analysed considering the TEG supply and a heating–cooling cycle. Figure 13 shows the converter output (red) and the regulated voltages (blue) from heating the TEG with a 250 ºC source and removing the source after the desired temperature is reached. Thus, one may determine the time interval for which the TEG+converter voltage is above 1.3 V, which is the minimum required by the LDO to ensure an output regulated at 1.2 V.

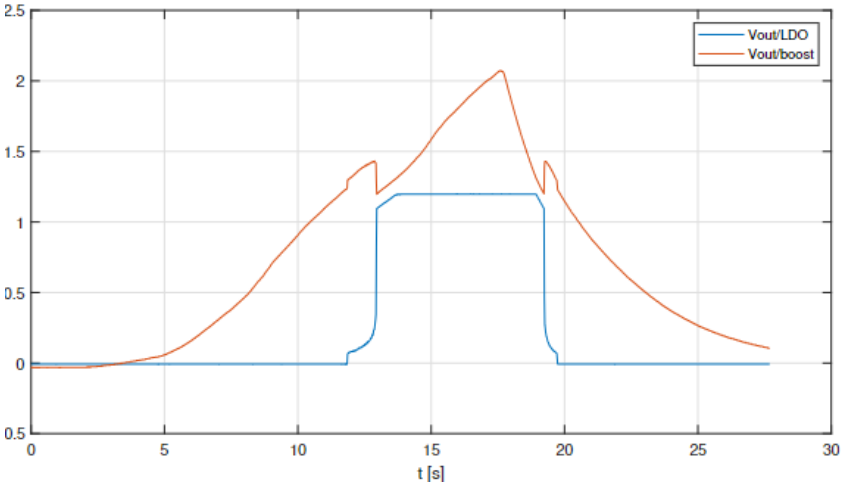

Figure 13. Converter output (red) and the regulated voltages (blue) after heating the TEG's hot plate with 250 ºC and subsequently removing the heat source.

As can be seen, the regulated 1.2 V output voltage is available for at least 6 s, considering this specific thermal system's inertia.

The supercapacitor's influence is analysed in Figure 14. Initially, it was applied to a temperature difference in the TEG that lasted twenty seconds. Then, the TEG was disconnected from the board by a push button. After the TEG was switched off, the output voltage on the LDO remained regulated for nearly 12 s, which is a sufficient period for several electronic system applications, as commented on in the Discussion section.

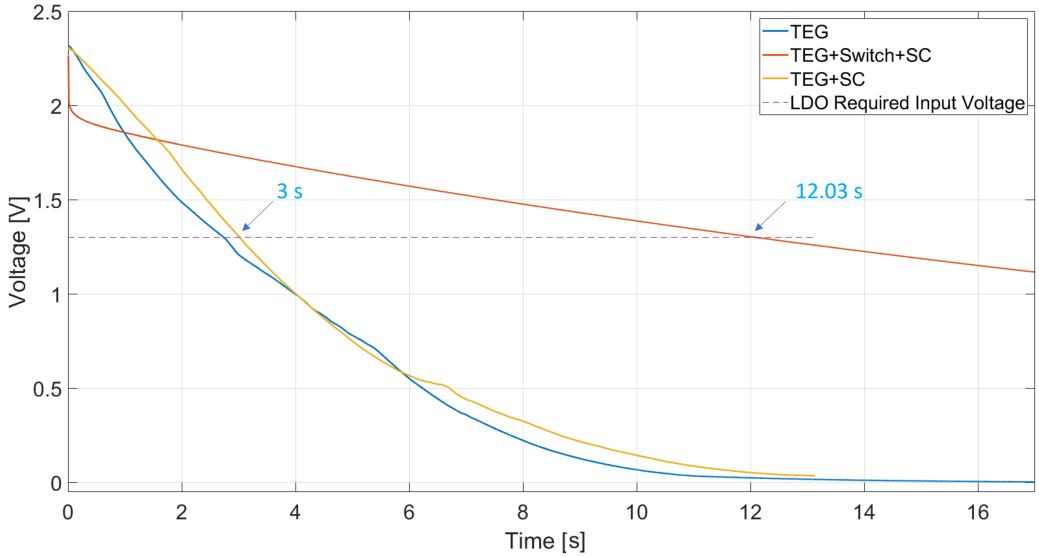

Figure 14. The influence of the supercapacitor on the system's fall time.

For a real application, there is no option to have a mechanical button. Thus, a diode is placed between the TEG and the supercapacitor, preventing the current from flowing back to the TEG. The direct consequence of this is a decrease in the boost input voltage for the same TEG temperature. The system without a supercapacitor lost more than half of its LDO active time (3 s to 1.43 s) in comparison with the solution without a diode, whereas the solution with a supercapacitor and diode only lost 27% of its on time (12.03 s to 8.52 s).

7. Discussion

Figure 12 confirms the correct design and experimental work of the proposed COTS component-based boost solution for energy harvesting applications. It must be noted that,

besides the ultra-low-voltage focus of this work, the system also performs efficiently, with an output voltage above 4.5 V, for supplies near 900 mV, which broadens its applications to the regulated standard value of 3.3 V.

Since, in this work, the hot plate temperature is not controlled, the output voltage is unregulated. In order to maintain a low level of circuit complexity and low component count, a solution resorting to a commercial voltage regulator was implemented instead of a complex control strategy. The results for a non-constant temperature are shown in Figures 14 and 15, proving the fulfilment of our research goals.

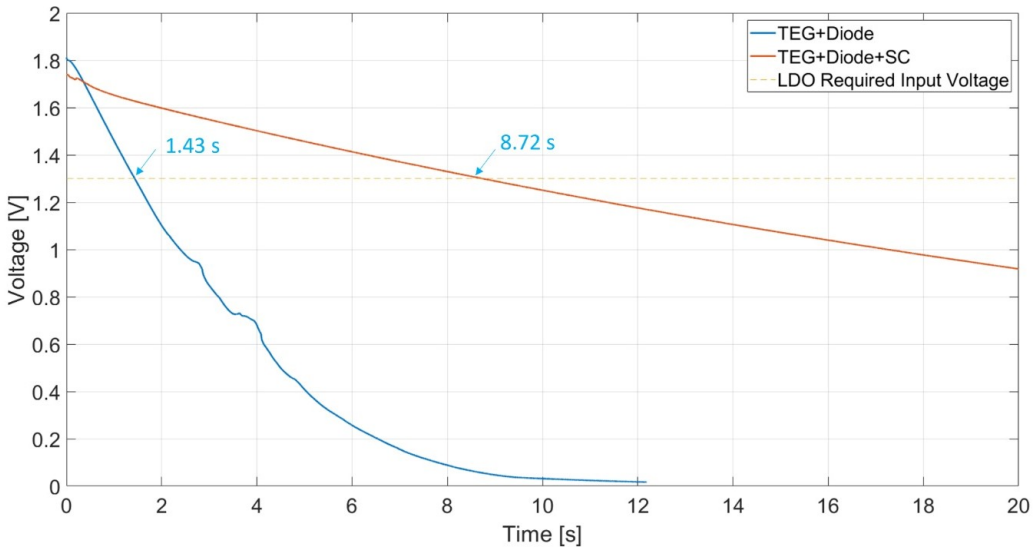

Figure 15. The influence of the supercapacitor on the system's fall time while adding the TEG-SC diode.

Experimentally, the TEG supply current is between 0.5 mA and 2.5 mA for the tested temperatures, resulting in a maximum power conversion efficiency of 75%. These attributes prove that it is possible to supply IoT nodes and wearable devices with a COTS-based solution using a maximum of 10 COTS components. Several strategies could be implemented in order to increase its power conversion efficiency and system features, for example, implementing a simple control strategy to increase the duty-cycle, D. Some solutions reported earlier in Table 1 present efficiencies similar to our proposal but resort to expensive CMOS-integrated solutions. The efficiency difference is mainly due to the oscillator selected to drive the boost MOSFETs. In fact, our selected LC oscillator generates a signal with less harmonics than the usual square wave. However, the inclusion of a CMOS inverter between the oscillator output and the boost MOSFET gate has two disadvantages: an increase in component count and power consumption.

This research work also demonstrates that this simple system architecture, resorting to COTS components, generates cost reduction at the expense of a negligible increase in area due to PCB prototyping.

Remote IoT node microcontrollers and their sensing and communication blocks will mostly be operating in sleep mode. Many remote IoT sensors already require µW to measure humidity, temperature, pressure, and air quality when active and at least ten times less power in sleep mode [5]. The same is true for the communication unit, whose power consumption depends on the protocol and frequency chosen. On average, some protocols already require power in µW, knowing that, most of the time, the unit is also in sleep mode [5]. According to [5], different communication protocols require different amounts of power and, due to their transmission rate, will need different time intervals to transmit or receive information. For instance, a Bluetooth protocol needs 210 mW for 1.5 s. However, if it is only active one time in 1 h, the average power is set at 700 µW. Similarly, ZigBee requires 2.5 mW for 4 s, which is the equivalent of 2 µW in an hour. The proposed

system delivers, for instance, 1.2 V for a load of 20 kΩ, leading to 72 μW, meaning that the proposed solution may deliver enough power for ZigBee communications and that it can become an add-on for Bluetooth applications.

Two main advantages to the proposed approach emerge when compared with the works presented in Table 1. Firstly, this solution allows internal circuit voltages above the CMOS component limits (for instance, 3.3 V considering CMOS 180 nm processes), leading to higher conversion ratios and output voltages of up to 5 V. On the other hand, due to circuit complexity, most of the works report start-up times of the order of hundreds of milliseconds, while our proposed direct MOSFET-driven LC oscillator permits a start-up time below 200 μs.

Also, the main idea of this research work is not the replacement of batteries with an energy harvester. In fact, these kinds of energy-autonomous systems could be combined with battery-powered system blocks. The goal is to propose solutions to reduce their ecological footprint by decreasing the number of replacements and battery charge cycles required.

Finally, the focus of this research was not efficiency, power density optimisation, setting new records, or designing the best power management system for remote IoT nodes. The idea was to show that by using general-purpose components and prioritising the component count, one may also ensure an energy conversion that may increase battery lifetime. This may also be achieved using second-life components, which also leads to an increase in ecological benefits.

8. Conclusions

This work proposes an inductor-based hard-switch boost converter to step up the voltage of a low-area TEG device (1.21 cm^2). The boost MOSFET's low-side switch is directly driven by an LC oscillator. The system is fabricated using multiple COTS device packages to fulfil the objective of reducing the component count and prototype cost. The final prototype area, including the TEG, is around 6 cm^2.

Our experimental results show that the system reaches output voltages of up to 5 V when the TEG hot plate reaches 250 ºC. The designed oscillator allows a start-up voltage of around 220 mV in just 150 μs.

The inclusion of the supercapacitor and diode at the input increases the operation period by 6 times (from 1.43 s to 8.72 s), allowing further data processing and communication in remote IoT nodes and portable devices.

As previously discussed, the proposed solution offers reasonable efficiency in comparison with CMOS-integrated solutions, together with the possibility of prototyping the system using low-cost COTS or second-life components.

Author Contributions: Conceptualization: P.M.d.S. and J.C.V.; methodology: P.M.d.S. and J.C.V.; formal analysis: P.M.d.S., J.C.V., R.A.M.L., J.P.N.T., and C.P.C.V.B.; investigation: J.A., P.M.d.S., J.C.V., R.A.M.L., J.P.N.T., and C.P.C.V.B.; writing—original draft preparation: J.A., P.M.d.S., and J.C.V.; writing—review and editing: P.M.d.S., R.A.M.L., and J.P.N.T.; supervision: P.M.d.S. and J.C.V.; project administration: P.M.d.S., R.A.M.L., and J.P.N.T.; funding acquisition: P.M.d.S., R.A.M.L., and J.P.N.T. All authors have read and agreed to the published version of the manuscript.

Funding: This research received no external funding.

Data Availability Statement: The original contributions presented in the study are included in the article, further inquiries can be directed to the corresponding author.

Acknowledgments: This work was supported in part by FCT/MCTES through national funds and in part by co-funded EU funds under Project UIDB/50008/2020. This work was also supported by FCT under the research grant UI/BD/151091/2021.

Conflicts of Interest: The authors declare no conflicts of interest.

References

1. Nozariasbmarz, A.; Collins, H.; Dsouza, K.; Polash, M.H.; Hosseini, M.; Hyland, M.; Liu, J.; Malhotra, A.; Ortiz, F.M.; Mohaddes, F.; et al. Review of wearable thermoelectric energy harvesting: From body temperature to electronic systems. *Appl. Energy* **2020**, *258*, 114069. [CrossRef]
2. Liu, H.; Zhao, C. Wearable electrochemical sensors for noninvasive monitoring of health-a perspective. *Curr. Opin. Electrochem.* **2020**, *23*, 42–46. [CrossRef]
3. Cekdin, C.; Nawawi, Z.; Faizal, M. The usage of thermoelectric generator as a renewable energy source. *Telkomnika* **2020**, *18*, 2186–2192. [CrossRef]
4. Bandyopadhyay, S.; Chandrakasan, A.P. Platform architecture for solar, thermal, and vibration energy combining with MPPT and single inductor. *IEEE J. Solid-State Circuits* **2012**, *47*, 2199–2215. [CrossRef]
5. Aldin, H.N.S.; Ghods, M.R.; Nayebipour, F.; Torshiz, M.N. A comprehensive review of energy harvesting and routing strategies for IoT sensors sustainability and communication technology. *Sens. Int.* **2024**, *5*, 100258. [CrossRef]
6. Tohidinejad, Z.; Danyali, S.; Valizadeh, M.; Seepold, R.; TaheriNejad, N.; Haghi, M. Designing a Hybrid Energy-Efficient Harvesting System for Head-or Wrist-Worn Healthcare Wearable Devices. *Sensors* **2024**, *24*, 5219. [CrossRef] [PubMed]
7. Romani, A.; Camarda, A.; Baldazzi, A.; Tartagni, M. A micropower energy harvesting circuit with piezoelectric transformer-based ultra-low voltage start-up. In Proceedings of the 2015 IEEE/ACM International Symposium on Low Power Electronics and Design (ISLPED), Rome, Italy, 22–24 July 2015; pp. 279–284.
8. Lu, T.; Wang, R.; Tang, Z.; Zou, Y.; Yue, X.; Liang, Y.; Gong, H.; Liu, S.; Chen, Z.; Liu, X.; et al. A Thermoelectric Energy Harvesting System Assisted by A Piezoelectric Transducer Achieving 10-mV Cold-Startup and 82.7% Peak Efficiency. *IEEE Trans. Power Electron.* **2024**, *39*, 6352–6363. [CrossRef]
9. Im, J.P.; Wang, S.W.; Ryu, S.T.; Cho, G.H. A 40 mV transformer-reuse self-startup boost converter with MPPT control for thermoelectric energy harvesting. *IEEE J. Solid-State Circuits* **2012**, *47*, 3055–3067. [CrossRef]
10. Chandrarathna, S.C.; Lee, J.W. A dual-stage boost converter using two-dimensional adaptive input-sampling MPPT for thermoelectric energy harvesting. *IEEE Trans. Circuits Syst. I Regul. Pap.* **2019**, *66*, 4888–4900. [CrossRef]
11. Kilani, D.; Mohammad, B.; Alhawari, M. Switched inductor DC–DC boost regulator using voltage-to-time controller for TEG applications. *Energies* **2022**, *15*, 3330. [CrossRef]
12. Noh, Y.S.; Seo, J.I.; Kim, H.S.; Lee, S.G. A reconfigurable DC-DC converter for maximum thermoelectric energy harvesting in a battery-powered duty-cycling wireless sensor node. *IEEE J. Solid-State Circuits* **2022**, *57*, 2719–2730. [CrossRef]
13. Bose, S.; Anand, T.; Johnston, M.L. Integrated cold start of a boost converter at 57 mV using cross-coupled complementary charge pumps and ultra-low-voltage ring oscillator. *IEEE J. Solid-State Circuits* **2019**, *54*, 2867–2878. [CrossRef] [PubMed]
14. Radin, R.L.; Sawan, M.; Galup-Montoro, C.; Schneider, M.C. A 7.5-mV-Input Boost Converter for Thermal Energy Harvesting with 11-mV Self-Startup. *IEEE Trans. Circuits Syst. II Express Briefs* **2019**, *67*, 1379–1383. [CrossRef]
15. Patra, S.; Sahu, S.; Abichandani, P.G.; Meshram, K.; Bhattacharya, S.; Muthe, K.; Prakash, D.; Singh, A. Self-operating flyback converter for boosting ultra-low voltage of thermoelectric power generator for IoT applications. *IEEE Trans. Ind. Electron.* **2021**, *69*, 12957–12966. [CrossRef]
16. Patra, S.; Muthe, K.P.; Singh, A. Low Voltage and Low Power Self-Startup Oscillator-Driven Boost Converter for Thermoelectric Generator Operating at Low Temperature. *IEEE Trans. Ind. Electron.* **2024**, *71*, 12457–12467. [CrossRef]
17. Patra, S.; Singh, A. Boost Converter Powered by Thermoelectric Generator to Harvest Low Temperature Waste Heat. In Proceedings of the 2024 Second International Conference on Smart Technologies for Power and Renewable Energy (SPECon), Ernakulam, India, 2–4 April 2024; pp. 1–6. [CrossRef]
18. Markiewicz, M.; Dziurdzia, P.; Konieczny, T.; Skomorowski, M.; Kowalczyk, L.; Skotnicki, T.; Urard, P. Software controlled low cost thermoelectric energy harvester for ultra-low power wireless sensor nodes. *IEEE Access* **2020**, *8*, 38920–38930. [CrossRef]
19. Chen, M.; Yu, H.; Wang, G.; Lian, Y. A batteryless single-inductor boost converter with 190 mV self-startup voltage for thermal energy harvesting over a wide temperature range. *IEEE Trans. Circuits Syst. II Express Briefs* **2018**, *66*, 889–893. [CrossRef]
20. dos Santos, P.M.; Serralheiro, A.J.; Borges, B.; Torres, J.P.N.; Charas, A. An Experimental Study on Step-Up DC–DC Converters for Organic Photovoltaic Cells. *J. Low Power Electron. Appl.* **2022**, *12*, 20. [CrossRef]